ACS OMEGA

http://pubs.acs.org/journal/acsodf

Article

Electrochemical Sensor for Detection and Degradation Studies of Ethyl Violet Dye

Rashida Yahya, Afzal Shah,* Tayyaba Kokab, Naimat Ullah, Muhammad Kamran Hakeem, Mazhar Hayat, Abdul Haleem, and Iltaf Shah*

Cite This: *ACS Omega* 2022, 7, 34154−34165

Read Online

ACCESS | Metrics & More | Article Recommendations | Supporting Information

ABSTRACT: In this work, a simple and sensitive electrochemical method was developed to determine ethyl violet (EV) dye in aqueous systems by using square wave anodic stripping voltammetry (SWASV) employing a glassy carbon electrode modified with acidic-functionalized carbon nanotubes (COOH-*f*CNTs). In square wave anodic stripping voltammetry, EV exhibited a well-defined oxidation peak at 0.86 V at the modified GCE. Impedance spectroscopy and cyclic voltammetry were used to examine the charge transduction and sensing capabilities of the modified electrode. The influence of pH, deposition potential, and accumulation time on the electro-oxidation of EV was optimized. Under the optimum experimental conditions, the limit of detection with a value of 0.36 nM demonstrates high sensitivity of COOH-*f*CNTs/GCE for EV. After detection, it was envisioned to devise a method for the efficient removal of EV from an aqueous system. In this regard a photocatalytic degradation method of EV using Ho/TiO_2 nanoparticles was developed. The Ho/TiO_2 nanoparticles synthesized by the sol−gel method were characterized by UV−vis, XRD, FTIR, SEM, and EDX. The photocatalytic degradation studies revealed that basic medium is more suitable for a higher degradation rate of EV than acidic and neutral media. The photodegradation kinetic parameters were evaluated using UV−vis spectroscopic and electrochemical methods. The results revealed that the degradation process of EV follows first-order kinetics.

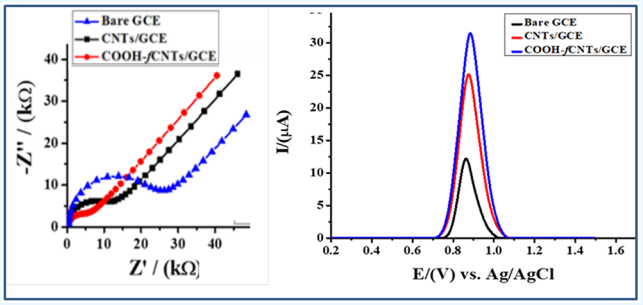

1. INTRODUCTION

In the present world, energy crises and pollution have become serious threats to humans and the environment. Industrialization and population expansion are major factors that contribute to environmental pollution and energy shortages.[1,2] With the advancement of industry, the overuse of chemicals and poisonous effluent discharge have become more significant contributors to degrading the natural environment.[3] The dumping of radioactive and nonbiodegradable industrial waste, the emission of hazardous gases, and contamination by toxic substances in the air and water pollute the entire ecosystem, leading to the extinction of marine life as well as serious respiratory and immune system health problems.[4,5] Contaminated drinking water is a serious threat to mankind and has become a political and social concern for nations around the world. Industrial wastewater includes dyes, pesticides, and nonbiodegradable organic and inorganic compounds.[6] The extensive use of various grades of chemical dyes to provide diverse colors in textiles, foodstuffs, and tanned products is the leading cause of drinking water pollution. Most of the dyes are carcinogenic and toxic to aquatic life, and their utilization produces waste that is released into the environment.[7−9]

Dyes released into the environment through wastewater are hazardous to aquatic life.[10] Owing to the hazardous effects of waste material dumped into the water by organic industries, it is essential to eliminate the waste and especially dyes. Due to the variability of their structural configuration, dyes such as anionic, cationic, naphtha-based, azo, acidic, basic, and metal complex dyes are chemically stable.[11] The toxicity and stability of these pollutants in the environment have become a complicated subject for regulatory bodies all over the world. Owing to their hazardous effects, it is essential to eliminate these dyes from drinking water. Dyes can be degraded photochemically, photocatalytically, or by using nanoparticles, enzymes, or bacteria.[12] For instance, ethyl violet dye, which is widely utilized in many industries, can be removed from the environment by biological treatment, adsorption, incineration, foam flotation, and/or photodegradation.[13,14] Modern electrochemical and spectroscopic techniques are more widely used for dyes monitering.[1]

Received: June 3, 2022
Accepted: August 30, 2022
Published: September 13, 2022

In this work, we used electrochemical and spectroscopic techniques to detect and degrade ethyl violet dye. Square wave voltammetry (SWV), one of the electrochemical techniques, is a fast detection method that generates signals of the targeted analyte with high resolution. By incorporating acidic-functionalized carbon nanotubes (COOH-*f*CNTs) to the working electrode surface, we developed an electrochemical sensor for electrochemical studies. The CNTs are cylindrical tubes made up of layers of coaxially produced graphene sheets that have a large surface area and attractive electrical properties.[15−17] Further, acidification of CNTs enhances the surface area and active sites to accommodate the analyte molecules. In addition, a photocatalytic study of ethyl violet dye was carried out using titanium oxide (TiO_2) nanostructure-based photocatalysts.[18] TiO_2 exhibits greater stability, recyclability, and chemical and physical inertness.[19] The low toxicity allows it to be used in broader applications in the food and medical fields, such as in dentistry, bone tissue engineering, and nanocarriers for drug delivery.[20,21] During photodegradation, its photocatalytic ability becomes lower due to recombination on photogenerated charge carriers.[22] Consequently, to delay the recombination of charge carriers, doping with rare earth elements has been carried out.[23] Holmium (Ho^{3+}) doped with TiO_2, ZnO, and CdS attracted the interest of scientists due to its unique structural and optical properties. These semiconductors show promise for photodegradation applications, as the doped elements hinder the charge carrier recombination process.[24,25] Therefore, Ho/TiO_2 nanoparticles can be used as a photocatalyst for the degradation of ethyl violet. Furthermore, TiO_2 is the most efficient, cost-effective photocatalyst and has a bandgap of 3.2 eV. Photocatalysis of ethyl violet dye relies on the creation of electron−hole pairs in TiO_2 NPs dispersed in aqueous medium by sufficient light energy, which breaks down the enlarged dye molecules.[26]

The work is novel, as the sensing platform has been employed for the first time to detect EV dye with a limit of detection down to 0.36 nM. The implementation of a smart approach to increase the GCE's conducting ability resulted in a lower limit of detection for larger molecular compounds such as EV. Another step which imparted more sensitivity to the electrode surface for the targeted analyte is that we drop-casted the dye on the designed modified electrode and dipped into the solution of supporting electrolyte of known concentration and pH. In this way, closer accessibility of the dye molecules to the electrode surface was achieved as witnessed by the robust current signal. This approach has resolved the orientation issue of the electroactive moiety. Improper orientation of the oxidizable moiety hinders the closer accessibility of the molecule, and consequently a poor signal is obtained when dye solution is placed in a electrochemical cell. Optimized conditions also significantly improve the limit of detection. Hence, we investigated the dye in various conditions and selected the best sensing conditions. Another unique feature of this research is that the designed sensor was used to examine the kinetics of EV degradation. The targeted dye was degraded using a synthesized photocatalyst (3% Ho-doped TiO_2 photocatalyst), and samples were taken at regular intervals and tested using the sensing platform. In this manner, the degradation was followed from the decrease in peak current height of EV. The degradation was also monitored spectrophotometrically by employing UV/vis spectroscopy. The dye was degraded up to 96%, and the degradation extent and kinetic results obtained from both techniques were found in close agreement. Hence, the developed method holds great promise for the treatment of dye-contaminated wastewater. This is the first report on an electroanalytical technique and designed sensor that demonstrates its uniqueness through considerable peak current magnification and plays an important role in dye degradation study. To the best of our knowledge, degradation monitoring of EV is not so far reported on an electrochemical sensor.

2. EXPERIMENTAL DETAILS

2.1. Reagents and Materials. All chemicals used during the experiment were purchased from Sigma-Aldrich, Merck, or Alfa Aesar and were of analytical grade. The COOH-*f*CNTs were used as a modifier, and ethyl violet was used as the analyte. Holmium-doped titanium oxide nanoparticles (Ho/TiO_2 NPs) were synthesized and characterized as a photocatalyst. The chemicals used for the synthesis of Ho/TiO_2 NPs were holmium(III) nitrate pentahydrate, titanium(IV) isopropoxide, and 2-propanol. Different kinds of supporting electrolytes, including HCl, H_2SO_4, phosphate-buffered solution (PBS), NaCl, Britton−Robinson buffer (BRB), KCl, and NaOH, were prepared using analytical grade reagents.

2.2. Instrumentation. A Metrohm Autolab PGSTAT302N device running with NOVA 1.11 software was used to carry out the electrochemical studies. The cell assembly comprised a three-electrode system in which AglAgCl (3.0 M KCl) was used as reference, platinum wire as counter, and modified glassy carbon electron (GCE) as working electrode. The photodegradation study of ethyl violet was performed on a Shimadzu UV-1700 spectrophotometer in the wavelength range of 200 to 800 nm.

2.3. Synthesis of Holmium-Doped TiO_2 NPs (Photocatalyst). Ho-doped TiO_2 NPs were synthesized by using the sol−gel technique. First, a specific amount (3%) of holmium(III) nitrate pentahydrate was dissolved in 200 g of 2-propanol and stirred until the holmium salt dissolved completely. To this solution was added 97 g of titanium(IV) isopropoxide (titanium precursor), and it was stirred for 10 min using a magnetic stirrer. As a result, we obtained an alkoxide solution. Then a mixture of 25.35 g of deionized water and 127 g of 2-propanol was prepared and added to the alkoxide solution dropwise. The mixture was stirred for 24 h at room temperature. Filtration was carried out, and then the precipitate was dried in an oven at 100 °C before being calcined in a muffle furnace at 500 °C.

2.4. Cleaning of the Working Electrode. Before the experiment, the surface of the glassy carbon electrode was cleaned physiochemically to activate it. A silver mirror-like surface of the electrode was accomplished by scrubbing the surface in a figure eight pattern on a pad with a 0.5 μm alumina slurry and rinsing it with distilled water.[27] Afterward, the cleaned electrode was chemically cleaned by dipping it in the supporting electrolyte while recording voltammograms at a scan rate of 100 mV/s in a potential window of 0 and 1.5 V. Voltammograms with no current variation indicated that the surface of the working electrode was clean.[28]

2.5. Preparation of the Modified Electrode. The GCE was modified through the layer-by-layer drop-casting method, by which modifier COOH-*f*CNTs were coated on the precleaned electrode surface. A 5 μL drop of COOH-*f*CNTs at a concentration of 1 mg/mL was drop-casted on the surface of the working electrode and air-dried. After that, a 5 μL drop of analyte (concn = 15 μM) was applied to the prepared sensor

https://doi.org/10.1021/acsomega.2c03472
ACS Omega 2022, 7, 34154−34165

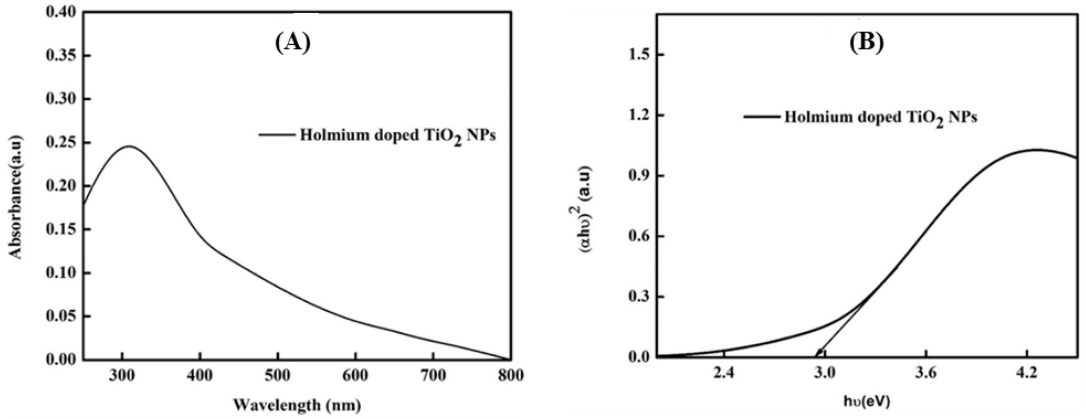

Figure 1. (A) UV−vis spectrum and (B) Tauc plot of 3% Ho/TiO_2 NPs.

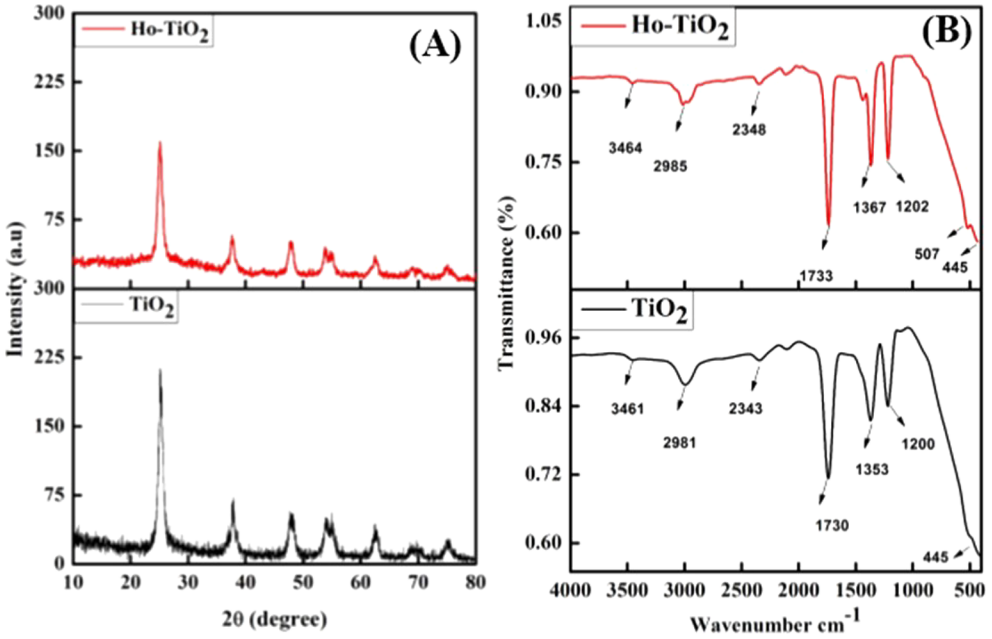

Figure 2. (A) XRD pattern and (B) FT-IR spectrum of 3% Ho/TiO_2 NPs.

and air-dried again. The prepared electrode was used for electroanalytical studies, with 0.1 M PBS used as supporting electrolyte to record cyclic and square wave voltammograms during the sensor performance evaluation.

3. RESULTS AND DISCUSSION

3.1. Characterization of Photocatalyst. *3.1.1. UV−Vis Spectrum Analysis.* The UV−vis spectrum of 3% Ho/TiO_2 NPs is shown in Figure 1A. The aqueous suspension of the synthesized sample reveals an absorption peak at 311 nm, with a fundamental absorption edge at 520 nm. The energy gaps of holmium-doped TiO_2 were calculated by using a Tauc plot (Figure 1B).

$$\alpha h\upsilon = A(h\upsilon - E_g)^n \quad (1)$$

where α denotes the absorption coefficient, h is the photon's energy, A is the proportionality constant, and n is the electronic transition with 3% Ho/TiO_2 NPs $n = 1/2$; therefore, the calculated band gap is 2.77 eV.[29,30]

3.1.2. XRD Spectrum Analysis. Figure 2A shows the XRD pattern of pristine and 3% Ho/TiO_2 NPs, which corresponds to JCPDS card number 00-001-0562. In 3% Ho/TiO_2 NPs XRD, peaks at $2\theta = 25.10°$, 37.91°, 48.10°, 54.79°, and 62.68° verify the same anatase structure as observed for pristine TiO_2.[31] No major peak shift was observed in XRD, verifying the successful substitution of doped metal oxide into the crystal lattice of TiO_2 to produce homogeneous Ho-doped TiO_2 nanoparticles. In addition, no further holmium peaks were detected in the synthesized sample, indicating the absence of any impurities. The average crystallite size of the sample was determined by using the Debye−Scherrer equation:[32]

$$D = \frac{K\lambda}{\beta \cos\theta} \quad (2)$$

where K indicates the Scherrer constant, β is full width at half-maximum, λ is the wavelength of light, and θ is Bragg's angle. The average crystallite size of 3% Ho/TiO_2 NPs was calculated to be 13.73 nm.[33]

3.1.3. FT-IR Spectrum Analysis. The FT-IR spectrum of pristine and 3% Ho/TiO_2 NPs in the 4000−400 cm^{-1} region. For doped material (Figure 2B), a bending mode of Ti−O−Ti

https://doi.org/10.1021/acsomega.2c03472
ACS Omega 2022, 7, 34154−34165

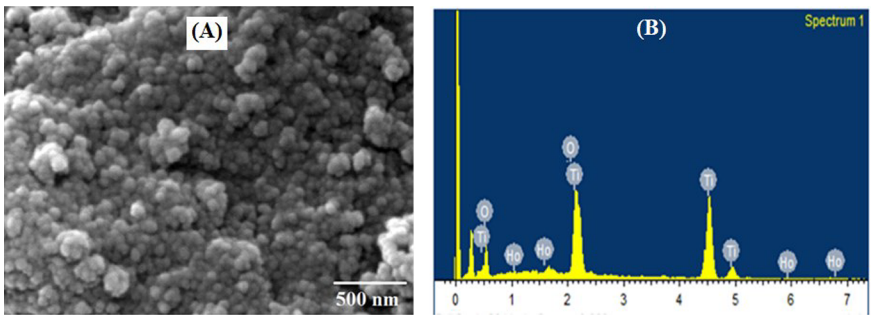

Figure 3. (A) SEM image and (B) EDX spectrum of 3% Ho/TiO_2 NPs.

at 900−400 cm^{-1} indicates an anatase phase of titania NPs. Likewise, the O−H stretching mode at 3464 and 1367 cm^{-1}, water adsorption peak at 1733 cm^{-1}, metal oxide (Ho−O and Ti−O bands) bending mode peak at 507 and 445 cm^{-1}, CO_2 and CO adsorption peak at 2356 cm^{-1},[34] and Ti−O−CH vibration peak at 3026 cm^{-1} verify the successful synthesis of 3% Ho/TiO_2 NPs.[25,35] Similar FT-IR signals were observed in pristine TiO_2 with the absence of a peak around 507 cm^{-1} which particularly corresponds to the Ho−O bond present in the doped material.

3.1.4. SEM and EXD Analysis. Scanning electron microscopy was studied to evaluate the morphological characteristics of the synthesized nanoparticles. A SEM image of 3% Ho/TiO_2 NP is shown in Figure 3A, where aggregated spherical 3% Ho/TiO_2 NPs can be seen at a magnification of 500 nm. Following XRD and FT-IR investigations which showed that both TiO_2 and Ho-TiO_2 NPs have tetragonal (anatase) structures, morphological analysis illustrated that doping further enhanced the particle shape and reduced agglomeration between the NPs. The elemental composition of 3% Ho/TiO_2 NPs was investigated by using energy-dispersive X-ray spectroscopy. The EDX result shown in Figure 3B reveals that Ti, Ho (holmium), and oxygen were present in the synthesized sample. An EDX table, revealing the quantification of holmium (Ho) dopant in TiO_2, is shown in Table 1.

Table 1. EDX Data Showing the Quantification of Holmium (Ho) Dopant in TiO_2

serial number	compound	wt % oxygen	wt % titanium	wt % dopant
1	Ho-TiO_2	60.81	36.43	2.76

3.2. Electrochemical Characterization. Electrochemical characterization of the defined sensing platform was performed using EIS and SWV techniques. EIS gives useful information regarding charge transfer properties at the sensor surface. The EIS measurement of COOH-*f*CNTs/GCE was carried out in a 5 mM $K_3[Fe(CN)_6]$ redox probe in 0.1 M KCl electrolyte at a frequency range of 14 kHz to 1 Hz. Figure 4A shows the Nyquist plots of bare and modified GCE. The largest semicircle diameter of bare GCE compared to COOH-*f*CNTs/GCE indicates a faster charge transfer at the COOH-*f*CNTs, while CNTs/GCE presents a charge transduction rate between COOH-*f*CNTs and bare GCE. The R_{ct} values obtained for CNTs/GCE (10.5 kΩ) and COOH-*f*CNTs/GCE (4.6 kΩ) are lower than that for bare glassy carbon electrode (22.11 kΩ). The smallest R_{ct} value of COOH-*f*CNTs/GCE indicate optimum charge transport of the developed sensor owing to an increased electroactive surface area.[36] The modifier imparts enhanced electrical properties to bare GCE by acting as a bridge between the analyte and the transducer.[37] The Randles equivalent circuit, shown in the inset of Figure 4a, was used to calculate R_{ct} and other EIS parameters, as listed in Table S1.

The cyclic voltammograms of the bare and modified GCE were obtained in a 5 mM $K_3[Fe(CN)_6]$ redox probe and 0.1 M KCl solution. The CV plots shown in Figure 4B were used to measure the active surface area of bare GCE, CNTs/GCE, and COOH-*f*CNTs/GCE by the Randles−Sevcik equation:

$$I_p = 2.69 \times 10^5 n^{3/2} A C_o D^{1/2} R v^{1/2} \quad (3)$$

For 5 mM $K_3[Fe(CN)_6]$, $n = 1$, $D = 7.6 \times 10^{-6}$ cm^2 s^{-1}, and v = 100 mV/s; thereby, the I_p value from CV was used to find the surface area as tabulated in Table S2. The surface area values indicate a 5 times higher surface area of COOH-*f*CNTs/GCE than bare GCE. The CV results verify the EIS data, and COOH-*f*CNTs/GCE was selected as a sensing platform for further investigation.

3.3. Voltammetric Analysis of the Targeted Analyte. Square wave voltammetry (SWV) was successfully applied for the detection of ethyl violet dye on the surface of modified GCE under optimized conditions. The square wave anodic stripping voltammograms were recorded on bare/GCE, CNTs/GCE, and HOOC-*f*CNTs/GCE by using 15 μM ethyl violet dye solution at a potential range of 0.2 to 1.5 V, PBS pH 6.0, scan rate 100 mV/s, deposition potential 0.5 V, and deposition time 5 s. Figure 5 shows the oxidation peak current of the targeted analyte on bare and modified GCEs. The peak current values were enhanced on CNTs/GCE and HOOC-*f*CNTs/GCE. The improved performance of CNTs and HOOC-*f*CNTs GCEs was attributed to the high surface area and superior catalytic activity of the designed sensor for the targeted analyte.[38] The results show that ethyl violet dye is oxidized at 0.87 V with an I_p of 12.12 μA on bare GCE, while the peak current was enhanced up to 25.06 and 31.40 μA on CNTs/GCE and HOOC-*f*CNTs/GCE, respectively. Therefore, acid-functionalized carbon nanotubes were chosen to develop an electrochemical sensor to detect ethyl violet dye.

3.4. Effect of Scan Rates. The effect of scan rates (25−150 mV/s) on the oxidation peak current of the analyte (Figure 6A) was studied by using cyclic voltammetry (CV). The cyclic voltammograms for ethyl violet dye were recorded in a potential window of −1.0 to 1.5 V. The anodic peak current was enhanced by increasing the scan rate. The relationship between scan rate and peak current provides information about the type of reaction (adsorption controlled or diffusion controlled) that occurred at the modified GCE surface. The I_p vs v plot with a correlation factor of 0.99

https://doi.org/10.1021/acsomega.2c03472
ACS Omega 2022, 7, 34154−34165

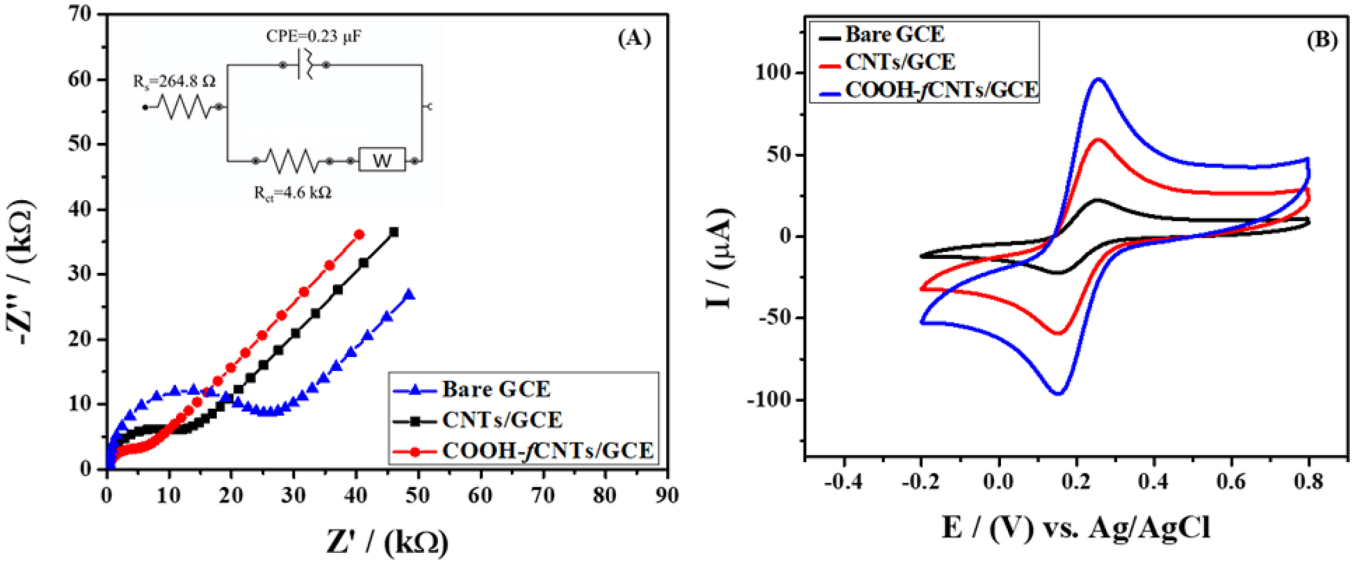

Figure 4. (A) EIS Nyquist plots and (B) cyclic voltammograms recorded in solution of 5 mM $K_3[Fe(CN)_6]$ and 0.1 M KCl on bare and modified GCE at a scan rate of 100 mV s^{-1}.

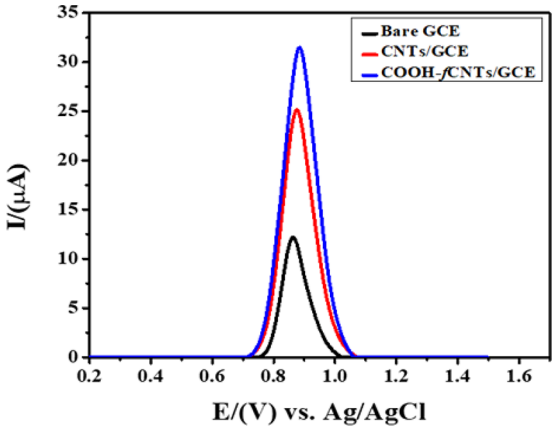

Figure 5. Comparative SWVs of 15 μM ethyl violet on bare GCE, CNTs/GCE, and HOOC-*f*CNTs/GCE in a supporting electrolyte of 0.1 M PBS (pH = 6) at a scan rate of 100 mV/s.

(Figure S1 A) is more linear than the I_p vs $v^{1/2}$ plot with a correlation coefficient of 0.97 (Figure S1 B). Thus, the reaction on the modified electrode surface was adsorption controlled, which was further confirmed by the log I_p vs log v plot, where the slope was nearly equal to 1 (Figure 6B), verifying surface-assisted reaction at the sensor surface.[39]

3.5. Optimization of Experimental Parameters.

Optimization of parameters including supporting electrolyte, pH of solution, deposition potential, and deposition time was performed at the designed sensor. The nature of the supporting electrolyte greatly affected the peak shape, position, and intensity of the desired analyte. To select the optimum supporting electrolyte, 0.1 M PBS, BRB, NaCl, KCl, and H_2SO_4 were checked. A well-defined peak shape and high peak current density were obtained with 0.1 M PBS electrolyte, as shown in Figure 7; thus, 0.1 M PBS was chosen as the best supporting electrolyte for detection of ethyl violet on HOOC-*f*CNTs/GCE.

SWV was performed at pH 3−12 to check the involvement of protons in the electrochemical oxidation of ethyl violet dye on COOH-*f*CNTs/GCE. The SW voltammograms in Figure 8A shows maximum signals at pH 6.0. The anodic peak shifting linearly toward the lower potential with increased pH of the

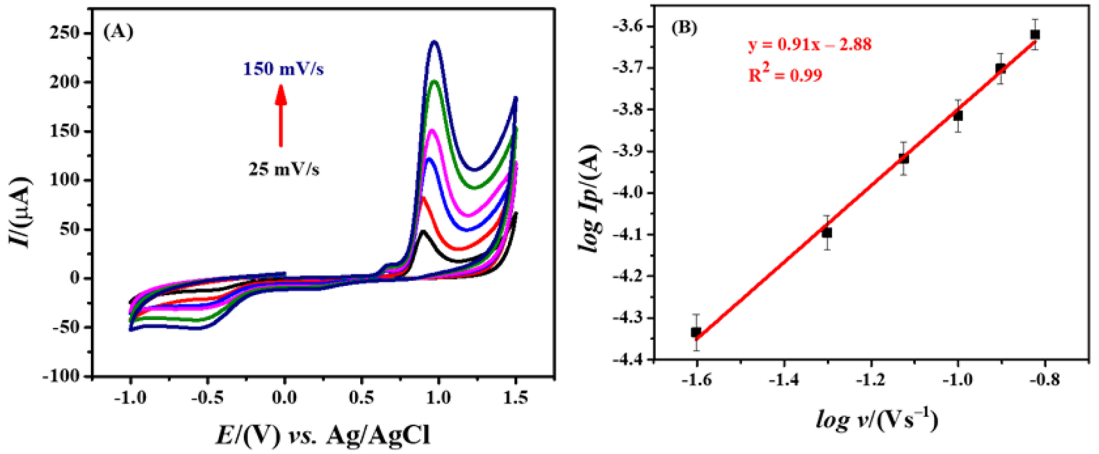

Figure 6. (A) Cyclic voltammograms of ethyl violet (15 μM) at various scan rates in PBS (pH = 6.0). (B) Plot of log I_p vs log v.

https://doi.org/10.1021/acsomega.2c03472
ACS Omega 2022, 7, 34154−34165

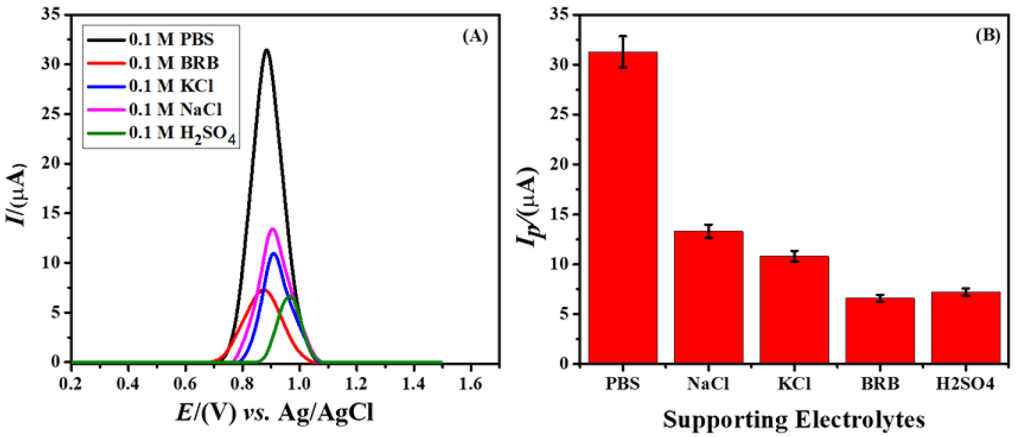

Figure 7. (A) Square wave voltammograms of ethyl violet (15 μM) on COOH-fCNTs/GCE in different supporting electrolytes at a scan rate of 100 mV/s, deposition potential of 0.5 V. (B) Bar graph of various supporting electrolytes vs peak current.

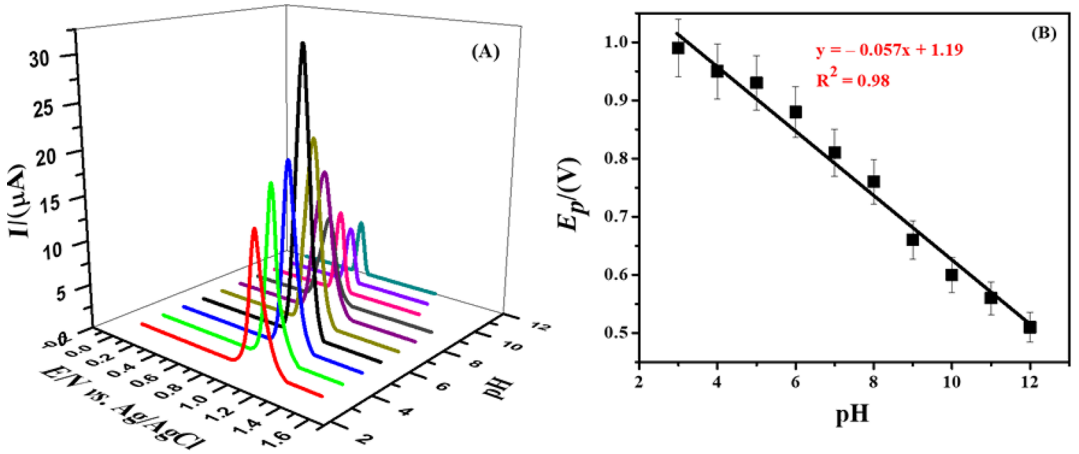

Figure 8. (A) SWV peak currents of 15 μM ethyl violet as a function of pH of PBS (3−12) obtained at a scan rate of 100 mV/s. (B) Calibration plot of E_p vs pH.

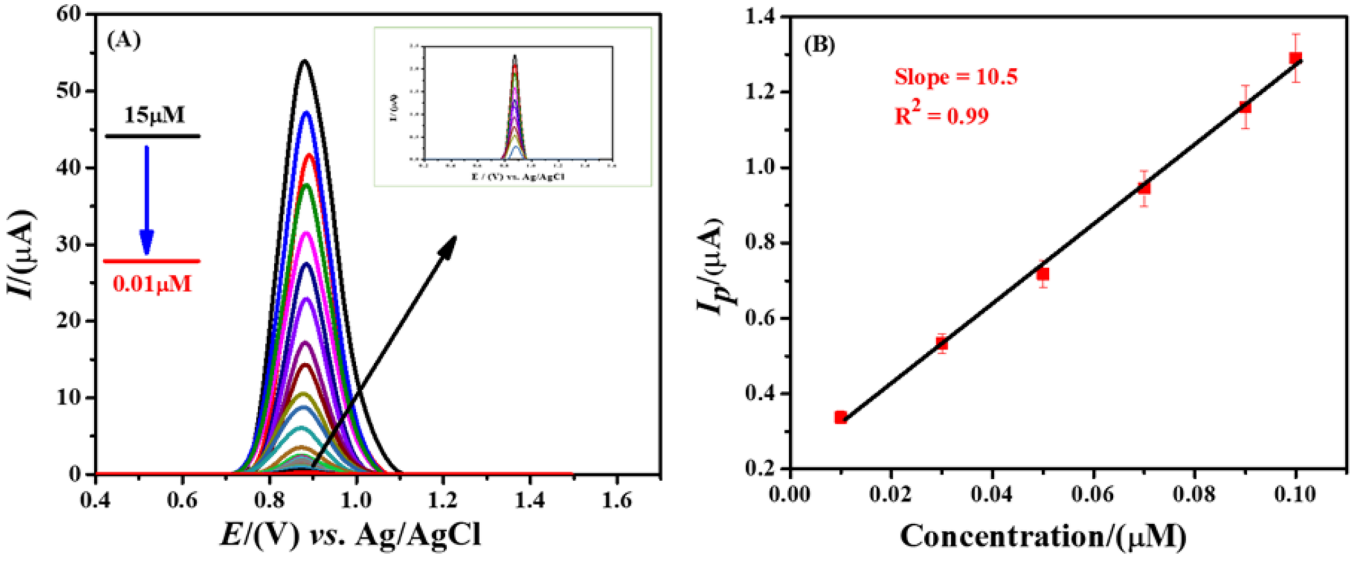

Figure 9. (A) SWV recorded for COOH-fCNTs/GCE by varying the concentration of ethyl violet in PBS at pH = 6.0, scan rate of 100 mV/s, deposition potential of −0.4 V, and deposition time of 5 s. (B) Calibration plots obtained by SWV data of a lower concentration range.

medium indicates the involvement of protons in the electrochemical process (Figure 8B). On the pH vs potential plot, the slope value 57 mV/pH (Figure 8B) is close to the Nernstian slope (59 mV/pH),[40] which indicates that equal numbers of electrons and protons were involved in the oxidation of ethyl violet. At the modified electrode, the fCNTs facilitate the

https://doi.org/10.1021/acsomega.2c03472
ACS Omega 2022, 7, 34154−34165

Table 2. Comparison between HOOC-*f*CNTs/GCE Assay and Other Reported Ethyl Violet Detection Methods

method	material	LOD (nM)	references
microcloud point extraction	Triton X-114	12	42
chemometric-assisted	HCl−KCl	22	43
surface-enhanced Raman scattering	Cu-nanoleaves	1×10^{-3}	44
surface-enhanced Raman scattering	PSi/Ag NPs	0.1	45
surface-enhanced Raman scattering	Ag@Cu@CW	10^{-1}	46
dispersive solid-phase extraction.	GO	9	47
electrochemiluminescence	CuS/GCE	3.2	48
electrochemical	COOH-*f*CNTs/GCE	0.36	this work

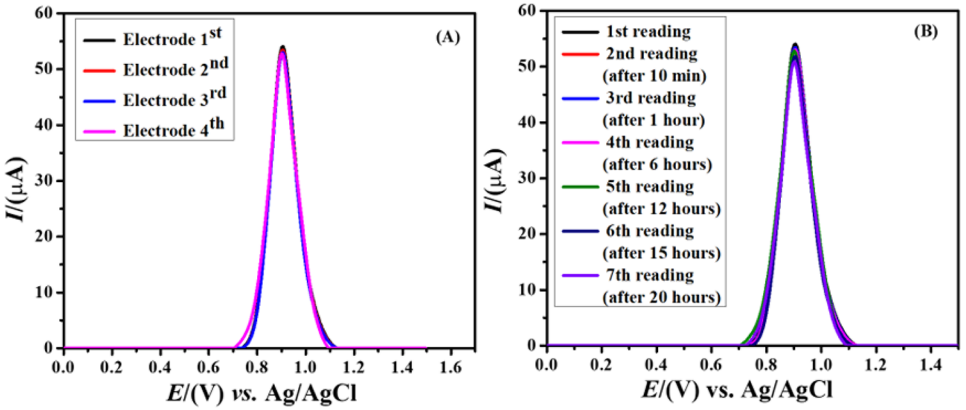

Figure 10. SW voltammograms showing (A) reproducibility and (B) repeatability of the developed sensor in 0.1 M PBS electrolyte at pH = 6.0, scan rate of 100 mV/s, deposition potential of −0.4 V, and deposition time of 5 s.

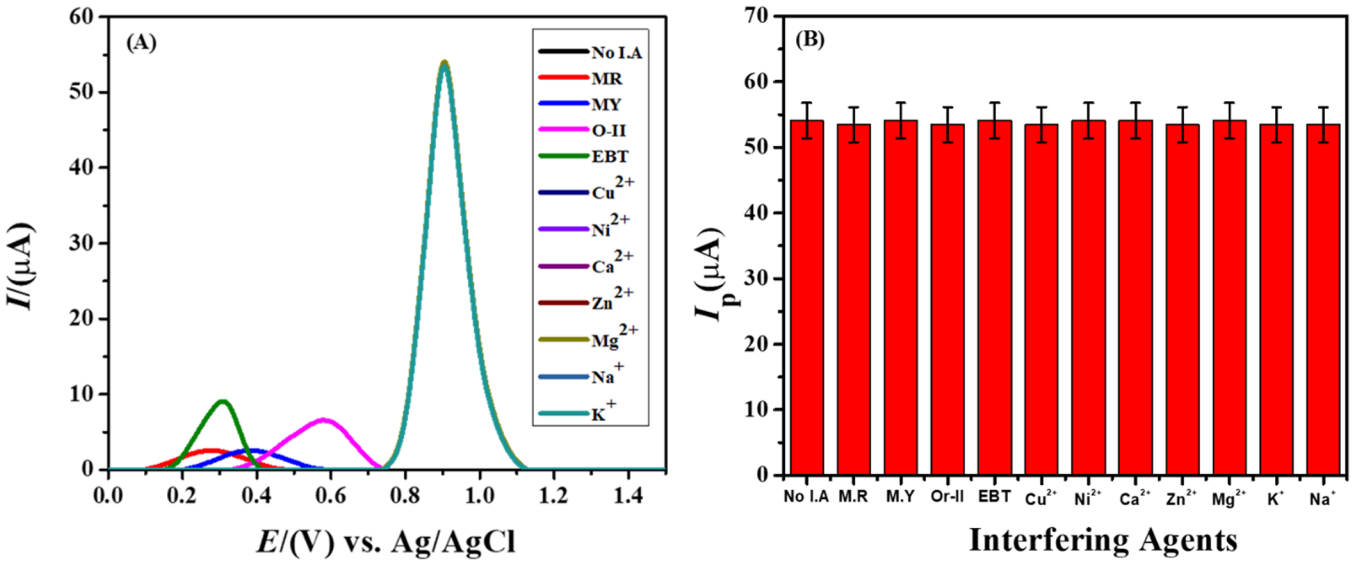

Figure 11. (A) Square wave voltammograms of 15 μM ethyl violet in the presence and absence of different interfering agents using 0.1 M PBS of pH 6.0. (B) Bar graph of the peak current of ethyl violet at the designed sensor.

electron transfer rate due to their conductive nature and support adsorption of EV during the preconcentration step of SWASV. Moreover, the oxygen functionalities of the *f*CNTs can develop hydrogen bonding with the EV nitrogen (H/N−H). In addition, the hydrogen bonds may also be developed between the surface-adsorbed analytes and their aqueous dissolved species. The rings of CNTs can offer additional $\pi-\pi$ interactions to the benzene unit of EV via solute−sorbent interactions to boost their regional concentration and enhance electrocatalytic redox events.

The effect of deposition potential and accumulation time was investigated by using SWV. Figure S2A and S2B shows the highest peak current at −0.4 V deposition potential, indicating that the maximum number of molecules of the dye were oriented for oxidation at this deposition potential. The optimum accumulation time to obtain the maximum dye molecule deposition on the sensor surface in 5 s is shown in Figure S3A and S3B.

3.6. Analytical Performance of HOOC-fCNTs/GCE. The performance of HOOC-*f*CNTs/GCE was analyzed by SWV under optimized conditions. The recorded voltammograms

https://doi.org/10.1021/acsomega.2c03472
ACS Omega 2022, 7, 34154−34165

Table 3. Real Sample Analysis of Ethyl Violet at the Designed Sensor under Optimized Conditions

dye	sample	initial amount (μM)	spiked amount (μM)	found (n = 4) (μM)	RSD (%)	recovery (%)
ethyl violet	industrial wastewater sample 1	0.0	15	14.5	2.2	98.33
	industrial wastewater sample 2	0.0	15	14.5	2.3	96.50
	fruit juice sample 1	0.0	15	14.80	2.8	96.00
	fruit juice sample 2	0.002	15	14.40 expected (15.002)	3.1	98.00
	hospital wastewater sample 1	0.005	15	14.9 expected (15.005)	3.4	96.36
	hospital wastewater sample 2	0.0	15	14.7	3.2	96.43

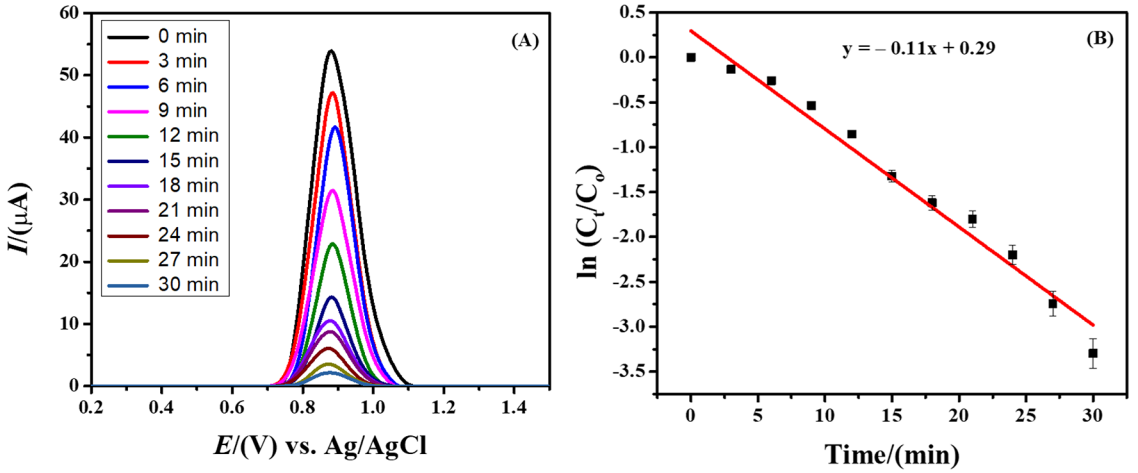

Figure 12. (A) Square wave voltammograms for degradation of ethyl violet solution were recorded for COOH-fCNTs/GCE in 0.1 M PBS electrolyte at pH = 6.0, scan rate of 100 mV/s, deposition potential of −0.4 V, and deposition time of 5 s. (B) Plot showing first-order kinetics.

with ethyl violet concentrations from 15 μM down to 0.01 μM are shown in Figure 9A. The limit of detection (LOD) of ethyl violet for the designed sensor was calculated according to IUPAC guidelines:[41] 3 σ/m, where m is the slope of a linear calibration plot (Figure 9B) and σ is the standard deviation of the blank solution. Based on peak current values of the blank solution (PBS, pH = 6.0), standard deviation was calculated for HOOC-fCNTs/GCE. The LOD of ethyl violet was found to be 0.36 nM, indicating that HOOC-fCNTs/GCE is a promising tool for trace level detection of targeted toxins. The calculated figures of merit especially the LOD value (0.36 nM) are far better than the reported LODs for the ethyl violet dye.[42−48] Table 2 shows a comparison between the HOOC-fCNTs/GCE assay and other reported ethyl violet detection methods. Remarkably, the LOD for the target analyte attainable by using the stated platform is much better than reported methods. A literature survey reveals that our designed electrochemical nanosensor is a preferred platform in the perspective of sensitivity, stability, and selectivity, indicating it as a promising tool for the level detection of targeted toxin.

3.7. Validity of the Designed Sensor. The validity of the designed sensor was confirmed by its reproducibility and repeatability. For this purpose, four electrodes were modified in the same way, and voltammograms were recorded under optimized conditions, as shown in Figure 10A. Identical peak current values of ethyl violet indicate good reproducibility of the designed sensor, with RSD < 5%. A repeatability experiment was performed by taking several readings on the same electrode, and the HOOC-fCNTs/GCE was found to be stable, with RSD < 5%, as shown in Figure 10B.

3.8. Study of the Effects of Interferents for Validation of the Designed Sensor. To find out the effect of interferents on the anodic peak response of the sensing platform, different dyes and metal ions at 1 mM were added individually as interferents to the 15 μM analyte solution. The interferents include dyes such as methyl red (MR), metanil yellow (MY), orange II (Or-II), and erichrome black T (EBT) along with metal ions such as Cu^{2+}, Ni^{2+}, Ca^{2+}, Zn^{2+}, Mg^{2+}, Na^{+}, and K^{+}. Under optimized conditions, the interfering species did not show any appreciable influence on the peak current response of EV as evident from Figure 11A. This behavior can be related to the strong affinity of the target analyte for the sensing platform. Signals for the interfering agents also appeared in the voltammogram along with the analyte's oxidation peak, but they had no discernible impact on the analyte's signal. These results confirm the EV selectivity of the sensing platform and its capability for detecting and identifying other dyes as well at potentials corresponding to their oxidation. The bar graph in Figure 11B suggests that the designed sensor has a % RSD value less than 3%, which points to its validity as a selective sensor. Thus, the designed sensing platform is capable of discriminating and sensing the target analyte from other species which may be present in real samples.

3.9. Application of the Sensor in Real Samples. A real analysis was carried out to analyze the designed modifier's precision and accuracy. For this purpose, the amounts of ethyl violet in industrial wastewater, fruit juice, and hospital wastewater samples were measured. Two milliliters of fruit juices was diluted to 10 mL by using 0.1 M PBS, and water samples were used as such. Initially, no contents of ethyl violet molecules were found in the real matrixes. Then a known amount of the targeted analyte was spiked by standard addition protocol. The recovered amount of ethyl violet was measured by using a calibration plot. All experiments were repeated four times, and the oxidation peak current corresponded to the I_p of

https://doi.org/10.1021/acsomega.2c03472
ACS Omega 2022, 7, 34154−34165

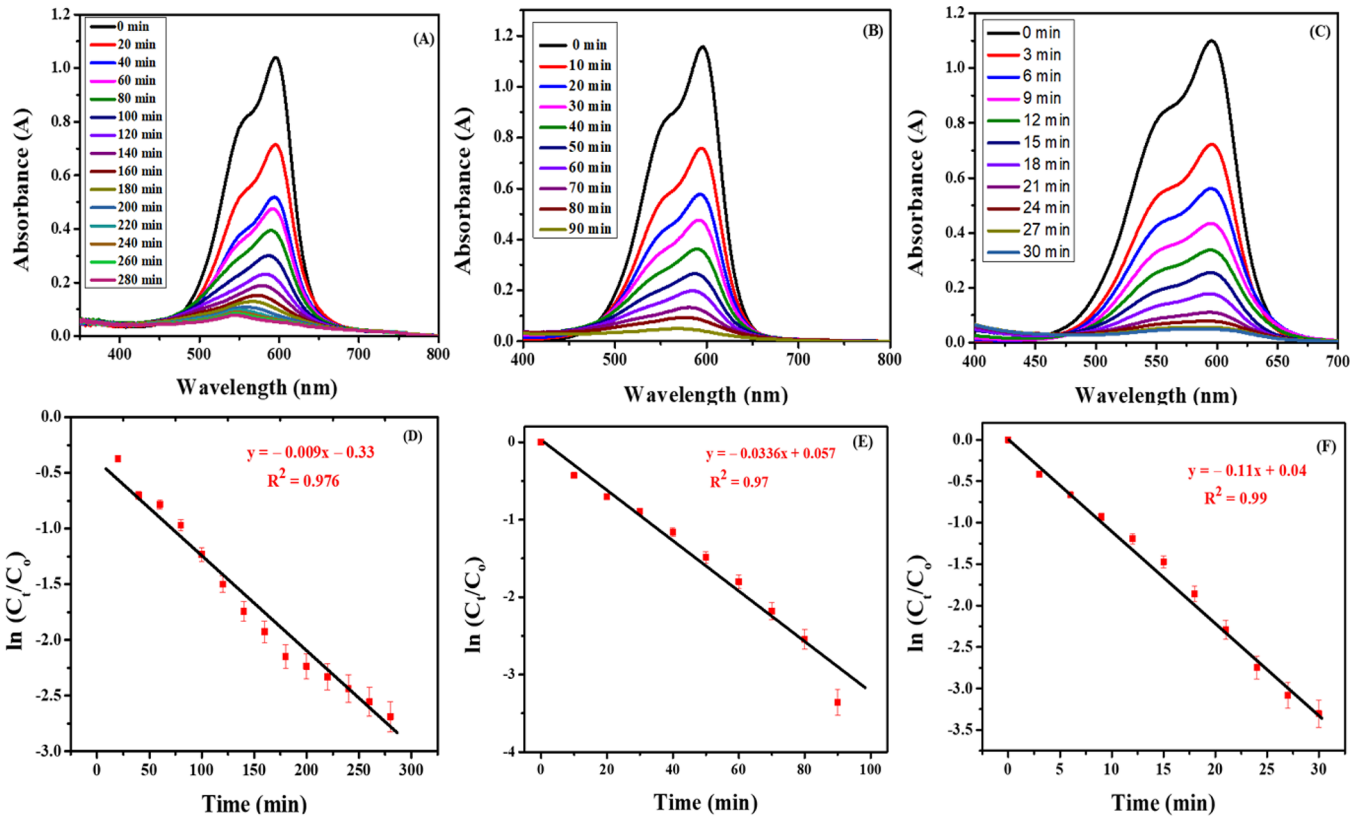

Figure 13. (A, D) UV−visible spectra and first-order kinetics plot of photocatalytic degradation of 15 μM ethyl violet dye at Ho/TiO_2 NPs in acidic medium. (B, E) UV−visible spectra and first-order kinetics plot of photocatalytic degradation of 15 μM ethyl violet dye at Ho/TiO_2 NPs in neutral medium. (C, F) UV−visible spectra and first-order kinetics plot of photocatalytic degradation of 15 μM ethyl violet dye at Ho/TiO_2 NPs in basic medium.

Figure 9. Table 3 reveals that the developed sensor is quite sensitive for ethyl violet dye with % RSD in the range of 2.2−3.4%. The percent recoveries of the targeted analyte in the range of 96.00−98.33% suggest the applicability of the designed sensor for real sample analysis.

3.10. Photodegradation Studies on the Designed Sensor. Photodegradation of ethyl violet with Ho/TiO_2 NP catalyst on the designed electrochemical sensor was studied under sunlight using an electrochemical system. For this purpose, 15 μM dye solution was prepared in aqueous (pH = 7.0), basic (pH = 13.0), and acidic (pH = 2.0) medium. The spectrophotometric study revealed that the rate of degradation was faster in basic medium. So, 0.1 mg of Ho/TiO_2 nanoparticles was added to a 50 mL basic solution of dye and stirred for 10 min as the maximum number of molecules of dye were adsorbed on the nanomaterial. Then 5 μL of dye solution was drop-casted on the HOOC-*f*CNTs/GCE and dried under hot air. The SW voltammogram was recorded as shown in Figure 12A. Then the basic solution of dye and NPs was kept under direct sunlight, and voltammograms were recorded every 3 min by repeating the same procedure as described above. The oxidation current gradually decreased as the concentration of dye in the solution decreased due to the breakdown of ethyl violet molecules. After 30 min, 96% of dye molecules had disappeared from the solution. The percent degradation and extent of reaction are shown in Figure S4A and S4B. A kinetic study was also carried out by plotting a first-order kinetic graph. The rate constant K was calculated by the slope of log $[I_p]_t/[I_p]_o$ vs time (min), as shown in Figure 12B.

3.11. Spectrophotometric Investigations of Photodegradation of Ethyl Violet. Photodegradation of ethyl violet dye was performed in sunlight by varying the pH conditions, as pH greatly affects the degradation rate by the production of H^+ and OH^- ions in the solution. The amount of H^+ and OH^- ions in the solution controls the interaction between dye molecules and surface charge of the catalysts.[49] The absorption spectra of ethyl violet in acidic, neutral, and basic media are shown in Figure 13A−C. The rate of degradation of ethyl violet dye molecules increased as the medium was changed from acidic to basic, as shown in Figure 13D−F. Higher alkalinity increased the degradation rate, as positively charged dye molecules are adsorbed more strongly on the surface of the Ho/TiO_2 photocatalyst through electrostatic forces.[50] The percent degradation was calculated by using the following formula:

$$\%\ \text{degradation} = \frac{C_o - C_t}{C_o} \times 100 \quad (4)$$

where C_o is the initial concentration of the dye solution and C_t is the concentration after irradiation with sunlight at time t. The order of reaction was estimated by ln C_t/C_o vs time plots. The rate constant (K) value was calculated from the slope: 0.009 min^{-1} in acidic, 0.033 min^{-1} in neutral, and 0.11 min^{-1} in basic medium. The percent degradation and extent of reduction in acidic, neutral, and basic media are shown in Figures S5−S7. The proposed photocatalytic degradation mechanism of ethyl violet can be seen in Schemes S1 and S2. This mechanism is consistent with literature reports.[51−53]

https://doi.org/10.1021/acsomega.2c03472
ACS Omega 2022, 7, 34154−34165

4. CONCLUSION

An effective electroanalytical technique based on COOH-*f*CNTs was developed for detecting ethyl violet in aqueous environments. The modifier played a mediating role in the charge transfer process at the interface of modified GCE and significantly improved the target analyte's current signals compared to bare GCE. The developed electrode presents excellent electrical features for analyte detection owing to its large electroactive surface area. To obtain exceptional sensitivity, experimental parameters including modifier concentrations, stripping electrolyte, medium pH, deposition potential, and accumulation period were optimized. Phosphate-buffered solution (PBS) was selected as the best electrolyte, because the highest peak current of the analyte on the designed electrode was obtained in PBS. The highest sensitivity of the sensor toward the analyte can be seen in its nanomolar level LOD value. Moreover, the photodegradation and decolorization of the analyte solution were also investigated using voltammetry and spectroscopic methods. The percent degradation of ethyl violet validates the claim that the proposed sensor has excellent performance and practical application in environmental water analysis.

■ ASSOCIATED CONTENT

Supporting Information

The Supporting Information is available free of charge at https://pubs.acs.org/doi/10.1021/acsomega.2c03472.

Table S1: Parameters obtained from equivalent circuit model. Table S2: Electroactive surface area of working electrodes. Figure S1: (A) Plot of oxidation peak current vs. scan rate. S1: (B) Plot of oxidation peak current vs. square root of scan rate. Figure S2: (A) Square wave anodic stripping voltammograms for optimum accumulation potential of ethyl violet dye (15 μM) using HOOC-*f*CNTs/GCE. S2: (B) Plot of I_p vs accumulation potential. Figure S3: (A) Selection of optimum deposition time for sensing of ethyl violet dye (15 μM) by using HOOC-*f*CNTs/GCE in 0.1 M PBS (pH = 6.0) with deposition potential of −0.4 V. S3: (B) Plot of I_p vs deposition time. Figure S4: (A) Plot of % degradation vs. time of ethyl violet on a designed sensor. S4 (B) plot of extent of reaction. Figure S5: (A) Plot of % degradation vs. Time of ethyl violet by using UV−visible spectroscopy in acid medium. S5: (B) plot showing extent of reaction. Figure S6: (A) Plot of % degradation vs. Time of ethyl violet by using UV−visible spectroscopy in neutral medium. S6: (B) plot of extent of reaction. Figure S7: (A) Plot of % degradation vs. Time of ethyl violet by using UV−visible spectroscopy in basic medium. S7: (B) plot of extent of reaction. Scheme S1. Proposed photocatalytic degradation pathway of the ethyl violet dye via destruction of conjugated structure. Scheme S2. Proposed photocatalytic degradation pathway of the ethyl violet dye through N-de-ethylation (PDF)

■ AUTHOR INFORMATION

Corresponding Authors

Afzal Shah − *Department of Chemistry, Quaid-i-Azam University, 45320 Islamabad, Pakistan;* orcid.org/0000-0002-9465-9185; Email: afzals_qau@yahoo.com

Iltaf Shah − *Department of Chemistry, College of Science, United Arab Emirates University, Al Ain, United Arab Emirates*; Email: altafshah@uaeu.ac.ae

Authors

Rashida Yahya − *Department of Chemistry, Quaid-i-Azam University, 45320 Islamabad, Pakistan*

Tayyaba Kokab − *Department of Chemistry, Quaid-i-Azam University, 45320 Islamabad, Pakistan*

Naimat Ullah − *Department of Chemistry, Quaid-i-Azam University, 45320 Islamabad, Pakistan*

Muhammad Kamran Hakeem − *Department of Chemistry, Quaid-i-Azam University, 45320 Islamabad, Pakistan*

Mazhar Hayat − *Department of Chemistry, Quaid-i-Azam University, 45320 Islamabad, Pakistan*

Abdul Haleem − *Department of Chemistry, Quaid-i-Azam University, 45320 Islamabad, Pakistan;* orcid.org/0000-0003-4034-6498

Complete contact information is available at: https://pubs.acs.org/10.1021/acsomega.2c03472

Author Contributions

Conceptualization, A.S., A.H., and R.Y.; methodology, R.Y., N.U. M.K.H., and M.H.; software, R.Y. and N.U.; validation, M.K.H., I.S., and A.S.; formal analysis, R.Y. and M.H.; investigation, R.Y. and N.U.; resources, I.S., A.S., and A.H.; data curation, T.K.; writing: original draft preparation, R.Y., N.U., M.H., M.K.H., and A.S; writing: review and editing, A.S., I.S., and T.K.; visualization, A.H., I.S., and M.H.; supervision, A.S.

Notes

The authors declare no competing financial interest.

■ ACKNOWLEDGMENTS

A.S. graciously acknowledges the generous support of Quaid-i-Azam University, Islamabad, Pakistan. I.S. graciously acknowledges the generous support of UAE University (Grant No: 12SO91 UPAR).

■ REFERENCES

(1) Pereira, J. C. Environmental issues and international relations, a new global (dis) order-the role of International Relations in promoting a concerted international system. *Rev. Bras. Polít. Int.* **2015**, *58*, 191−209.

(2) Nweke, O. C.; Sanders, W. H., III. Modern environmental health hazards: a public health issue of increasing significance in Africa. *Environ. Health Perspect.* **2009**, *117*, 863−870.

(3) Owa, F. Water pollution: sources, effects, control and management. *Environ. Health Perspect.* **2013**, *4*, 65−65.

(4) Dastoorpoor, M.; Sekhavatpour, Z.; Masoumi, K.; Mohammadi, M. J.; Aghababaeian, H.; Khanjani, N.; Hashemzadeh, B.; Vahedian, M. Air pollution and hospital admissions for cardiovascular diseases in Ahvaz. *Sci. Total Environ.* **2019**, *652*, 1318−1330.

(5) Schwarzenbach, R. P.; Egli, T.; Hofstetter, T. B.; Von Gunten, U.; Wehrli, B. Global water pollution and human health. *Annu. Rev. Environ. Resour.* **2010**, *35*, 109−136.

(6) Khan, F. S. A.; Mubarak, N. M.; Tan, Y. H.; Khalid, M.; Karri, R. R.; Walvekar, R.; Abdullah, E. C.; Nizamuddin, S.; Mazari, S. A. A comprehensive review on magnetic carbon nanotubes and carbon nanotube-based buckypaper for removal of heavy metals and dyes. *J. Hazard. Mater.* **2021**, *413*, 125375.

(7) Tkaczyk, A.; Mitrowska, K.; Posyniak, A. Synthetic organic dyes as contaminants of the aquatic environment and their implications for ecosystems: A review. *Sci. Total Environ.* **2020**, *717*, 137222.

(8) Tan, C.; Zhu, G.; Hojamberdiev, M.; Lokesh, K. S.; Luo, X.; Jin, L.; Zhou, J.; Liu, P. Adsorption and enhanced photocatalytic activity of the {0001} faceted Sm-doped $ZnIn_2S_4$ microspheres. *J. Hazard. Mater.* **2014**, *278*, 572−583.
(9) Rashid, T. U.; Kabir, S. F.; Biswas, M. C.; Bhuiyan, M. R. Sustainable wastewater treatment via dye−surfactant interaction: a critical review. *Ind. Eng. Chem. Res.* **2020**, *59*, 9719−9745.
(10) Chiu, Y. H.; Chang, T. F. M.; Chen, C. Y.; Sone, M.; Hsu, Y. J. Mechanistic insights into photodegradation of organic dyes using heterostructure photocatalysts. *J. Catal.* **2019**, *9*, 430.
(11) Marimuthu, S.; Antonisamy, A. J.; Malayandi, S.; Rajendran, K.; Tsai, P. C.; Pugazhendhi, A.; Ponnusamy, V. K. Silver nanoparticles in dye effluent treatment: A review on synthesis, treatment methods, mechanisms, photocatalytic degradation, toxic effects and mitigation of toxicity. *J. Photochem. Photobiol. B: Biol.* **2020**, *205*, 111823.
(12) Mani, S.; Bharagava, R. N. Exposure to crystal violet, its toxic, genotoxic and carcinogenic effects on environment and its degradation and detoxification for environmental safety. *Rev. Environ. Contam. Toxicol* **2016**, *237*, 71−104.
(13) Vyavahare, G.; Sutar, S.; Gurav, R.; Patil, R.; Patil, D.; Jadhav, J., Application of Biochar for the Treatment of Textile Dyes and Wastewater. In *Biochar and its Application in Bioremediation*; Springer, 2021, pp 169−191.
(14) Basuli, U.; Chattopadhyay, S.; Nah, C.; Chaki, T. K. Electrical properties and electromagnetic interference shielding effectiveness of multiwalled carbon nanotubes-reinforced EMA nanocomposites. *Polym. Compos.* **2012**, *33*, 897−903.
(15) Porwal, M.; Rastogi, V.; Kumar, A. An overview on carbon nanotubes. *MOJ. Bioequiv. Availab.* **2017**, *3*, 114−116.
(16) Giddaerappa; Manjunatha, N.; Shantharaja; Hojamberdiev, M.; Sannegowda, L. K. Tetraphenolphthalein Cobalt (II) Phthalocyanine Polymer Modified with Multiwalled Carbon Nanotubes as an Efficient Catalyst for the Oxygen Reduction Reaction. *ACS Omega* **2022**, *7*, 14291−14304.
(17) Suresh, R.; Rajendran, S.; Kumar, P. S.; Vo, D. V. N.; Cornejo-Ponce, L. Recent advancements of spinel ferrite based binary nanocomposite photocatalysts in wastewater treatment. *Chemosphere* **2021**, *274*, 129734.
(18) Danish, M. S. S.; Estrella, L. L.; Alemaida, I. M. A.; Lisin, A.; Moiseev, N.; Ahmadi, M.; Nazari, M.; Wali, M.; Zaheb, H.; Senjyu, T. Photocatalytic applications of metal oxides for sustainable environmental remediation. *Met.* **2021**, *11*, 80.
(19) Wang, Y.; Ding, L.; Yao, C.; Li, C.; Xing, X.; Huang, Y.; Gu, T.; Wu, M. Toxic effects of metal oxide nanoparticles and their underlying mechanisms. *Sci. Chin. Mater.* **2017**, *60*, 93−108.
(20) Morones, J. R.; Elechiguerra, J. L.; Camacho, A.; Holt, K.; Kouri, J. B.; Ramírez, J. T.; Yacaman, M. J. The bactericidal effect of silver nanoparticles. *Nanotechnol.* **2005**, *16*, 2346.
(21) Gupta, K.; Singh, R.; Pandey, A.; Pandey, A. Photocatalytic antibacterial performance of TiO_2 and Ag-doped TiO_2 against S. aureus. P. aeruginosa and E. coli. *Beilstein J. Nanotechnol.* **2013**, *4*, 345−351.
(22) Ayon, S. A.; Billah, M. M.; Nishat, S. S.; Kabir, A. Enhanced photocatalytic activity of Ho^{3+} doped ZnO NPs synthesized by modified sol-gel method: An experimental and theoretical investigation. *J. Alloys Compd.* **2021**, *856*, 158217.
(23) Haider, A. J.; Jameel, Z. N.; Taha, S. Y. Synthesis and characterization of TiO_2 nanoparticles via sol-gel method by pulse laser ablation. *Eng. Technol. J.* **2015**, *33*, 761−771.
(24) Parnicka, P.; Grzyb, T.; Mikolajczyk, A.; Wang, K.; Kowalska, E.; Steinfeldt, N.; Klein, M.; Mazierski, P.; Zaleska-Medynska, A.; Nadolna, J. Experimental and theoretical investigations of the influence of carbon on a Ho^{3+}-TiO_2 photocatalyst with Vis response. *J. Colloid Interface Sci.* **2019**, *549*, 212−224.
(25) Clavero, C. Plasmon-induced hot-electron generation at nanoparticle/metal-oxide interfaces for photovoltaic and photocatalytic devices. *Nat. Photonics* **2014**, *8*, 95−103.
(26) Naseri, A.; Majidi, M. Cheap and easy modification of glassy carbon electrode for voltammetric determination of dopamine in the presence of ascorbic acid. *DARU: Journal of Faculty of Pharmacy, Tehran University of Medical Sciences* **2011**, *19*, 270.
(27) Manzoor, A.; Kokab, T.; Nawab, A.; Shah, A.; Siddiqi, H. M.; Iqbal, A. Electrochemical detection of mercuric (II) ions in aqueous media using glassy carbon electrode modified with synthesized tribenzamides and silver nanoparticles. *RSC Adv.* **2022**, *12*, 1682−1693.
(28) Islam, M. A.; Haither, M. J.; Khan, I.; Islam, M. Optical and structural characterization of TiO_2 nanoparticles. *IOSR J. Electr. Electron. Eng.* **2012**, *3*, 18−24.
(29) Ullah, N.; Shah, S. M.; Hussain, H.; Ansir, R.; Hussain, M. N. Pyrocatechol violet sensitized Ho-TiO_2/ZnO nanostructured material: as photoanode for dye sensitized solar cells. *Mater. Res. Express* **2020**, *7*, 035003.
(30) Crepaldi, E. L.; Soler-Illia, G. J. d. A.; Grosso, D.; Cagnol, F.; Ribot, F.; Sanchez, C. Controlled formation of highly organized mesoporous titania thin films: from mesostructured hybrids to mesoporous nanoanatase TiO_2. *J. Am. Chem. Soc.* **2003**, *125*, 9770−9786.
(31) Manikandan, V.; Palai, A. K.; Mohanty, S.; Nayak, S. K. Eosin-Y sensitized core-shell TiO_2-ZnO nano-structured photoanodes for dye-sensitized solar cell applications. *J. Photochem. Photobiol. B: Biol.* **2018**, *183*, 397−404.
(32) Wu, J. C. S.; Chen, C. H. A visible-light response vanadium-doped titania nanocatalyst by sol−gel method. *J. Photochem. Photobiol. A: Chem.* **2004**, *163*, 509−515.
(33) Margan, P.; Haghighi, M. Hydrothermal-assisted sol−gel synthesis of Cd-doped TiO_2 nanophotocatalyst for removal of acid orange from wastewater. *J. Sol-Gel Sci. Technol.* **2017**, *81*, 556−569.
(34) Haider, A. J.; Jameel, Z. N.; Taha, S. Y. Synthesis and characterization of TiO_2 nanoparticles via sol-gel method by pulse laser ablation. *Eng. Technol. J.* **2015**, *33*, 761−771.
(35) Filippo, E.; Carlucci, C.; Capodilupo, A. L.; Perulli, P.; Conciauro, F.; Corrente, G. A.; Gigli, G.; Ciccarella, G. Enhanced photocatalytic activity of pure anatase TiO_2 and Pt-TiO_2 nanoparticles synthesized by green microwave assisted route. *Mater. Res.* **2015**, *18*, 473−481.
(36) Rajawat, D. S.; Srivastava, S.; Satsangee, S. P. Electrochemical determination of mercury at trace levels using eichhornia crassipes modified carbon paste electrode. *Int. J. Electrochem. Sci.* **2012**, *7*, 11456−11469.
(37) Sierra-Rosales, P.; Toledo-Neira, C.; Squella, J. Electrochemical determination of food colorants in soft drinks using MWCNT-modified GCEs. *Sens. Actuators B: Chem.* **2017**, *240*, 1257−1264.
(38) Tang, Y. Y.; Chen, P. Y. Gold Nanoparticle-electrodeposited Electrodes Used for p-Nitrophenol Detection in Acidic Media: Effect of Electrodeposition Parameters on Particle Density, Size Distribution, and Electrode Performance. *J. Chin. Chem. Soc.* **2011**, *58*, 723−731.
(39) Zahid, A.; Lashin, A.; Rana, U. A.; Al-Arifi, N.; Ullah, I.; Dionysiou, D. D.; Qureshi, R.; Waseem, A.; Kraatz, H. B.; Shah, A. Development of surfactant based electrochemical sensor for the trace level detection of mercury. *Electrochim. Acta* **2016**, *190*, 1007−1014.
(40) Patel, B. R.; Hassan, Q.; Noroozifar, M.; Kerman, K. Simultaneous Square Wave Voltammetric Detection of Endocrine-Disrupting Agents Using a Nanocomposite of Magnetic Fe_3O_4 Nanorods and Poly(3,4-methylenedioxy)aniline. *ACS Sustain. Chem. Eng.* **2020**, *8*, 15108−15119.
(41) Belter, M.; Sajnóg, A.; Barałkiewicz, D. Over a century of detection and quantification capabilities in analytical chemistry−Historical overview and trends. *Talanta* **2014**, *129*, 606−616.
(42) Ghasemi, E.; Kaykhaii, M. Application of Micro-cloud point extraction for spectrophotometric determination of Malachite green, Crystal violet and Rhodamine B in aqueous samples. *Spectrochim. Acta Part A: Mol. Biomol. Spectrosc.* **2016**, *164*, 93−97.
(43) Yu, S.; Yuan, X.; Yang, J.; Yuan, J.; Shi, J.; Wang, Y.; Chen, Y.; Gao, S. A chemometric-assisted method for the simultaneous determination of malachite green and crystal violet in water based on absorbance−pH data generated by a homemade pH gradient

https://doi.org/10.1021/acsomega.2c03472
ACS Omega 2022, 7, 34154−34165

apparatus. *Spectrochim. Acta Part A: Mol. Biomol. Spectrosc.* **2015**, *150*, 403−408.
(44) Xu, D.; Zhang, Y.; Zhang, S.; Yang, W.; Wang, Z.; Li, J. Copper nanoleaves SERS substrates with high surface roughness for sensitive detection crystal violet and rhodamine 6G. *Opt. Laser Technol.* **2022**, *145*, 107502.
(45) Harraz, F. A.; Ismail, A. A.; Bouzid, H.; Al-Sayari, S.; Al-Hajry, A.; Al-Assiri, M. Surface-enhanced Raman scattering (SERS)-active substrates from silver plated-porous silicon for detection of crystal violet. *Appl. Surf. Sci.* **2015**, *331*, 241−247.
(46) Yan, X.; Wang, M.; Sun, X.; Wang, Y.; Shi, G.; Ma, W.; Hou, P. Sandwich-like Ag@ Cu@ CW SERS substrate with tunable nanogaps and component based on the Plasmonic nanonodule structures for sensitive detection crystal violet and 4-aminothiophenol. *Appl. Surf. Sci.* **2019**, *479*, 879−886.
(47) Razi-Asrami, M.; Ghasemi, J. B.; Amiri, N.; Sadeghi, S. J. Simultaneous spectrophotometric determination of crystal violet and malachite green in water samples using partial least squares regression and central composite design after preconcentration by dispersive solid-phase extraction. *Environ. Monit. Assess.* **2017**, *189*, 1−14.
(48) Lan, Q.; Li, Q.; Zhang, X.; Chen, Z. A novel electrochemiluminescence system of CuS film and $K_2S_2O_8$ for determination of crystal violet. *J. Electroanal. Chem.* **2018**, *810*, 216−221.
(49) Pirsaheb, M.; Hossaini, H.; Nasseri, S.; Azizi, N.; Shahmoradi, B.; Khosravi, T. Optimization of photocatalytic degradation of methyl orange using immobilized scoria-Ni/TiO_2 nanoparticles. *J. Nanostructure Chem.* **2020**, *10*, 143−159.
(50) Wen, K.; Wei, L.; Ren, Z.; Wang, B.; Lu, J. Enhanced photocatalytic degradation of cationic and anionic dyes by Ag-modified g-C_3N_4 composite: Insights on different mechanisms under visible light. *J. Mater. Res.* **2021**, *36*, 1549−1560.
(51) Chen, C. C. Degradation pathways of ethyl violet by photocatalytic reaction with ZnO dispersions. *J. Mol. Catal. A Chem.* **2007**, *264*, 82−92.
(52) Lee, W. L. W.; Lu, C. S.; Lin, H. P.; Chen, J. Y.; Chen, C. C. Photocatalytic degradation of ethyl violet dye mediated by TiO_2 under an anaerobic condition. *J. Taiwan Inst. Chem. Eng.* **2014**, *45*, 2469−2479.
(53) Mai, F. D.; Lee, W. L. W.; Chang, J. L.; Liu, S. C.; Wu, C. W.; Chen, C. C. Fabrication of porous TiO_2 film on Ti foil by hydrothermal process and its photocatalytic efficiency and mechanisms with ethyl violet dye. *J. Hazard. Mater.* **2010**, *177*, 864−875.

https://doi.org/10.1021/acsomega.2c03472
ACS Omega 2022, 7, 34154−34165